Structural Control on Clay Mineral Authigenesis in Faulted Arkosic Sandstone of the Rio do Peixe Basin, Brazil

Ingrid B. Maciel [1], Angela Dettori [2], Fabrizio Balsamo [2,*], Francisco H.R. Bezerra [1,3], Marcela M. Vieira [3], Francisco C.C. Nogueira [4], Emma Salvioli-Mariani [2] and Jorge André B. Sousa [5]

[1] Post-Graduation Program on Geodynamics and Geophysics, Universidade Federal do Rio Grande do Norte, Natal, RN 59078-970, Brazil; ingridbmaciel@gmail.com (I.B.M.); bezerrafh@geologia.ufrn.br (F.H.R.B.)
[2] Department of Chemistry, Life Sciences and Environmental Sustainability, University of Parma, I-43124 Parma, Italy; angela.dettori@studenti.unipr.it (A.D.); emma.salviolimariani@unipr.it (E.S.-M.)
[3] Department of Geology, Federal University of Rio Grande do Norte, Natal, RN 59078-970, Brazil; marcela@geologia.ufrn.br
[4] Department of Petroleum Engineering, Federal University of Campina Grande, Campina Grande, PB 58100-000, Brazil; aulascezar@gmail.com
[5] Petrobras Research Center—CENPES, Rio de Janeiro, RJ 21941-915, Brazil; jorgeabs@petrobras.com.br
* Correspondence: fabrizio.balsamo@unipr.it; Tel.: +39-0521-905365

check for updates

Abstract: Clay minerals in structurally complex settings influence fault zone behavior and characteristics such as permeability and frictional properties. This work aims to understand the role of fault zones on clay authigenesis in arkosic, high-porosity sandstones of the Cretaceous Rio do Peixe basin, northeast Brazil. We integrated field, petrographic and scanning electron microscopy (SEM) observations with X-ray diffraction data (bulk and clay-size fractions). Fault zones in the field are characterized by low-porosity deformation bands, typical secondary structures developed in high-porosity sandstones. Laboratory results indicate that in the host rock far from faults, smectite, illite and subordinately kaolinite, are present within the pores of the Rio do Peixe sandstones. Such clay minerals formed after sediment deposition, most likely during shallow diagenetic processes (feldspar dissolution) associated with meteoric water circulation. Surprisingly, within fault zones the same clay minerals are absent or are present in amounts which are significantly lower than those in the undeformed sandstone. This occurs because fault activity obliterates porosity and reduces permeability by cataclasis, thus: (1) destroying the space in which clay minerals can form; and (2) providing a generally impermeable tight fabric in which external meteoric fluid flow is inhibited. We conclude that the development of fault zones in high-porosity arkosic sandstones, contrary to other low-porosity lithologies, inhibits clay mineral authigenesis.

Keywords: fault zones; deformation bands; clay authigenesis; shallow diagenesis

1. Introduction

Clay minerals have important economic applications in industry—e.g., [1]. Additionally, in most geological settings clay minerals can occur in faults, thus influencing their permeability, frictional properties [2–8] and subsurface fluid flow [4,9–14]. Therefore, the understanding of the feedback between faulting and clay mineral authigenesis has important implications for seismicity, the migration and accumulation of oil and gas in the subsurface, and contaminant transport in aquifers.

Faults in high-porosity sandstones are generally considered as barriers to fluid flow, due to the combined effect of grain size and porosity reduction within fault cores and associated deformation bands in damage zones [15–22]. In this context, clay minerals are commonly described as mechanically weak minerals, and because of this weakness their presence in faults commonly contributes to stable sliding failures [23,24]. Furthermore, the origin and distribution of clays in sandstone are also important in oil industry, because these minerals contribute to increases in the sealing potential of faults and can determine reservoir compartmentalization [3,6,8].

Several studies have described the clay mineralogy of fault zones [24–26], however little attention has been paid to the role of faults in determining the type and amount of clay mineral transformation in faulted, arkosic sandstones. The goal of this study is to investigate how fault zones in arkosic sandstones (composed of a fault core surrounded by deformation bands) modify grain-scale fabric and control clay mineral authigenesis at shallow burial depths. We selected the Cretaceous Rio do Peixe basin in northeast Brazil (Figure 1) as a case study, due to its excellent exposures of undeformed sandstones and well-preserved fault zones. By integrating field analysis with laboratory data, we conclude that deformation-band faulting in arkosic, high-porosity sandstones inhibits clay mineral authigenesis, rather than promoting alteration and clay mineral formation.

2. Geological Background of the Rio do Peixe Basin

The Rio do Peixe basin (RPB) is a pull-apart Early Cretaceous basin situated in northeastern Brazil. The basin was generated during the reactivation of Precambrian basement shear zones during the opening of the South Atlantic Ocean [27–30]. The basin's deeper depocenters were established based on gravity data, and reach depths of ~2420 m [30]. These depocenters are filled by continental siliciclastic sedimentary units which were deposited in fluvial and lacustrine depositional systems. These deposits are divided into three main stratigraphic units, namely, from the base to the top: (1) the Antenor Navarro Formation, represented by conglomerates and mudstones; (2) the Sousa Formation, composed of mudstones; and (3) the Rio Piranhas Formation, composed of conglomerates and coarse sandstones [31–33].

The Antenor Navarro Formation is the basal unit. It represents the main fill of the basin and contains typical syn-rift deposits. The formation consists of siliciclastic fluvial deposits that are exposed in large and continuous outcrops in different sectors of the basin (Figure 1). The sandstones and conglomerates are composed of quartz, feldspars, rock fragments and biotite. Their matrix consists of silt and dark brown clay (approximately 1–1.5%) [34]. The Souza Formation is the intermediate unit and consists mostly of mudstones and a few occurrences of sandstones and marls. These units were deposited in floodplains or shallow lakes on meandering rivers. The Rio Piranhas Formation is the top unit and consists of conglomerates and coarse sandstones interfingered with sandy mudstones [32].
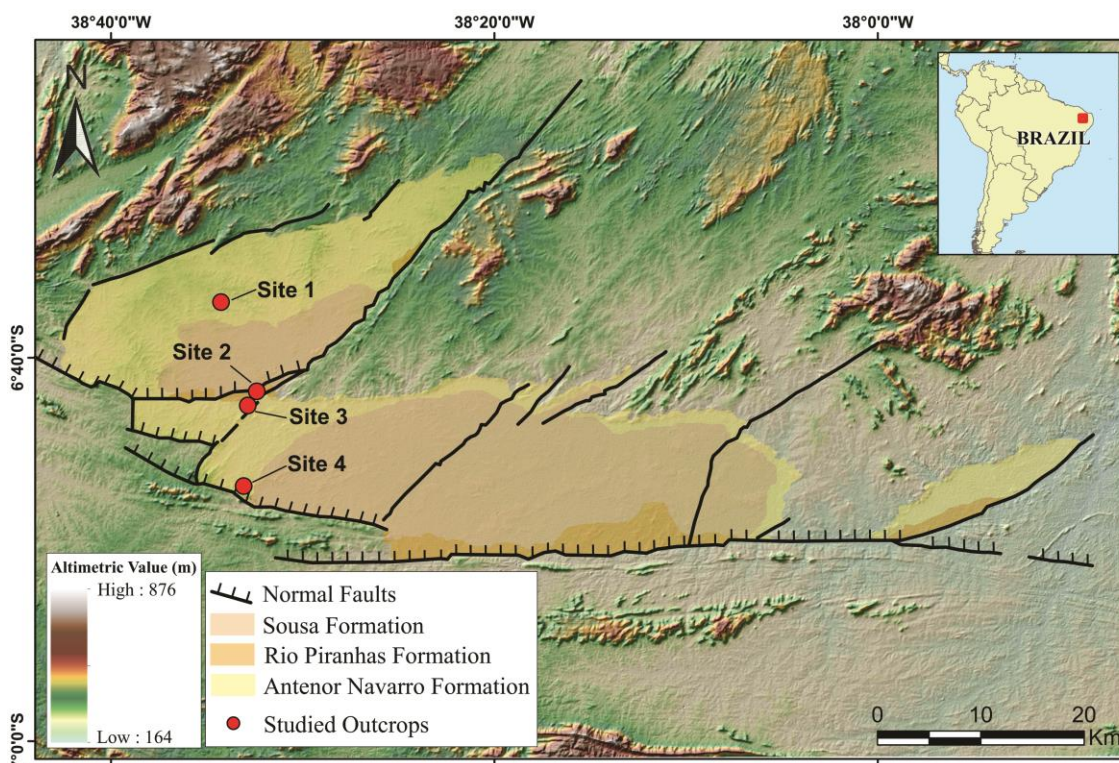
Figure 1. Simplified geological map of the Rio do Peixe Basin, showing major faults and the lithostratigraphics units. The location of the four selected outcrops is indicated. Modified from [27,29,35].

The sedimentary rocks of the Rio do Peixe basin were affected by two main tectonic phases: an Early to Late Cretaceous NW–SE oriented extension [29] followed by a basin inversion in a strike–slip regime from the Late Cretaceous to Cenozoic [35]. The extensional faults that developed during the first phase are dominated by deformation bands, often associated with slickensided surfaces [34]. The deformation bands occur as cm-thick tabular structures developed in the fault damage zone, and are arranged as single elements or in clusters. Within deformation bands, a cataclastic foliation was formed by preferential grain alignment and the selective fragmentation of feldspar grains [34].

3. Methods and Materials

This study focused on the western side of the Rio do Peixe basin, both in its central part far from major faults and in the proximity of the basin-boundary faults (Figure 1). Field analysis and sampling were performed at four main outcrops: one represents undeformed host rocks (Site 1) and the other three are deformed sites near major faults (Sites 2, 3 and 4). Site 1 is located in the undeformed part of the basin, where the basal Antenor Navarro sandstones are not affected by faults and fractures. In this site, we constructed a vertical sedimentary log to characterize the undeformed rocks. Sites 2 and 3 are located along the major intra-basinal fault zones in the Rio Piranhas sandstones and conglomerates, and are characterized by abundant fault zones with meter-scale offsets. Site 4 is located in the hanging wall block of the major basin-boundary fault in the Antenor Navarro sandstones, and has a displacement of ~170 m [36].

In the studied field sites, we collected a total of 95 samples of undeformed and faulted rocks, from which we made 34 thin sections. In the lab, we examined the following materials: (1) undeformed sandstones and conglomerates (i.e., host rocks); (2) deformed rocks collected within the fault zones, consisting of both deformation bands (single or clustered) and foliated cataclasites (see Section 4.1 for a description of fault zone structure). Thin section analysis was performed using an optical microscope, and scanning electron microscopy (SEM) combined with energy dispersive spectroscopy (EDS). The thin sections were impregnated with stained blue epoxy to highlight porosity. For observations

using the light petrographic microscope, we focused on grain size and roundness, sorting, packing, porosity, mineral composition and amount of clay. We also described depositional and diagenetic features in undeformed and faulted samples. Small representative samples were analyzed using a scanning electron microscope (SUPERSCAN SSX-550, Shimadzu Corporation, Kyoto, Japan) to improve clay mineral identification and textural analysis. EDS was used to identify the main chemical elements and mineral composition of the samples. X-ray diffraction (XRD) analyses were performed using a Bruker (Billerica, MA, USA) D2 Phaser powder diffractometer (CuKα radiation, voltage of 30 kV, current of 10 mA, step size of 0.018, interval of 1 s per step) on powdered bulk samples (n = 10) and fraction samples <2 μm in size (n = 6) for clay mineral identification in undeformed and faulted rocks. The oriented samples of the clay fractions were analyzed under three different conditions: air dried; ethylene glycol saturated; and heated to a temperature of 550 °C. The powdered bulk samples were measured in the range 2–80° 2θ, and the clay fraction samples were measured in the range 2–20° 2θ. Mineral phase identification and semi-quantitative estimations were performed using the DIFFRAC.EVA suite software provided by Bruker Corporation (Billerica, MA, USA). The results of the XRD analyses, together with sample description and location, are listed in Table 1.

4. Results

4.1. Fault Zone Structure

The studied fault zones exhibit three major structural domains (Figure 2): (1) the host rock, i.e., the undeformed sandstone and conglomerates without any significant deformational features; (2) the fault core, where most of the fault slip is accommodated; and (3) the surrounding footwall and hanging wall damage zones, interposed between the host rock and fault core, and composed of deformation bands.
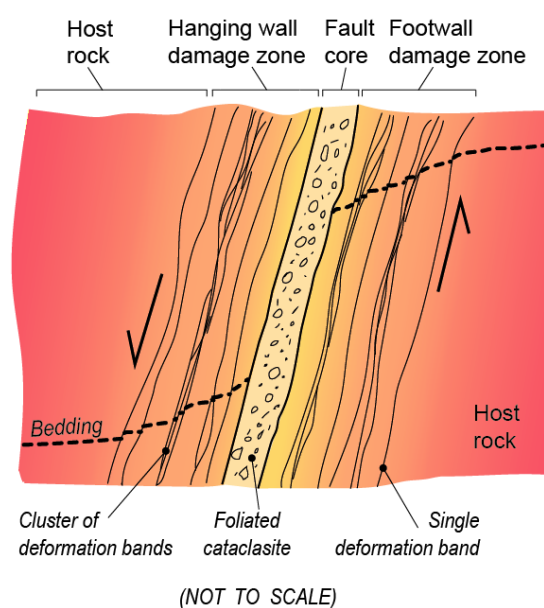

Figure 2. Conceptual sketch showing the typical architecture of fault zones in the Rio do Peixe basin. The host rock represents the sandstones and conglomerates with pristine textures and sedimentary structures not affected by faults. The fault core is the most deformed part of the fault zone, where slip surfaces were frequently developed and where several movements (different slicken lines) are observed. The damage zone is the deformed rock volume next to the fault core that has single or clusters of deformation bands (Sites 2, 3 and 4 in this study). Colors are indicative of the amount of weathering observed in the field.

Concerning the host rock, the original undeformed fluvial facies of the Rio do Peixe basin exhibit a massive laminated structure with trough–festoon crossbedding stratification (Figure 3). These units vary from silty sandstones to fine conglomerates. In a few cases, thin silt lenses are also observed (Figure 3). The sandstones are generally clast-supported with a granular texture, and grains are locally fractured. The grain sizes vary between silt and gravel.
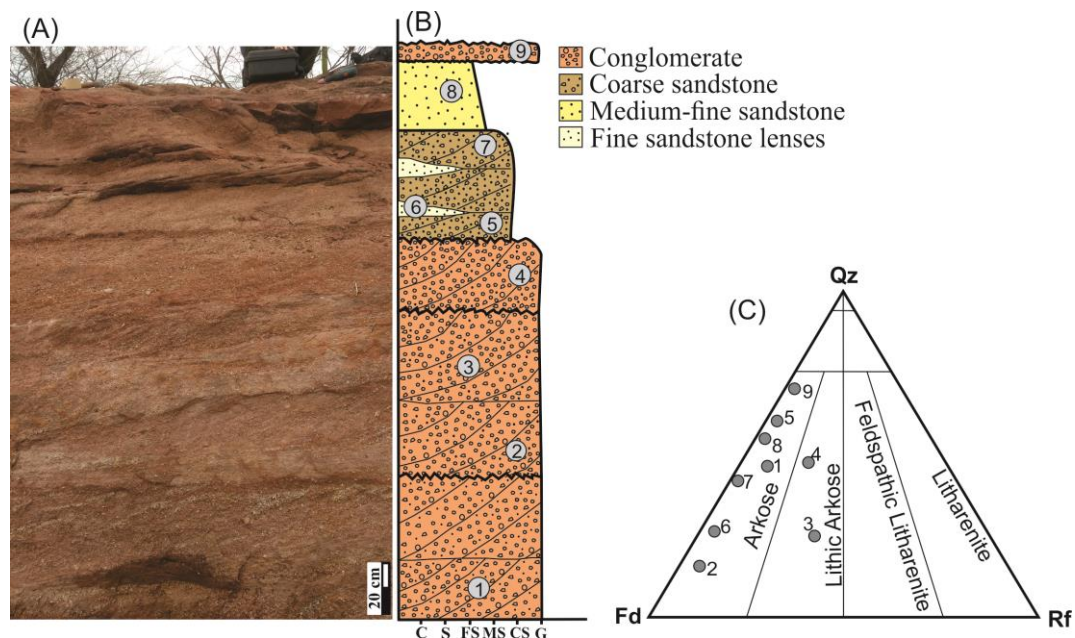

Figure 3. Schematic profile and compositional classification of the host rock (Antenor Navarro Formation) in the Rio do Peixe basin, Site 1. (**A**) Outcrop photograph showing fluvial sedimentary structures with tabular and lenticular shapes of fine sandstones and trough–festoon conglomerates. Note the intense red-orange coloration of undeformed rocks. (**B**) Vertical sedimentary log showing sampling position (Samples 1 to 9) in the fluvial succession. (**C**) Compositional classification of analyzed Samples 1 to 9, based on [37]. Key: c—clay; s—sand; fs—fine sand; ms—medium sand; cs—coarse sand; g—gravel; Qz—quartz; Fd—feldspar; Rf—rock fragments.

The fault cores range from 0.1 m to 0.3 m in thickness, whereas the width of the damage zones broadly range from ~5 m to 10 m (in small faults of Sites 2 and 3) up to ~200 m (in the hanging wall damage zone of Site 4). The fault cores and the inner damage zone generally form topographic relief up to 1 m in height with respect to the surrounding undeformed rock (Figure 4A). The sandstones in the fault core show a strong decrease in grain size and a preferential grain alignment, which forms a tectonic foliation visible at the hand scale (Figure 4B). Most offsets are extensional or slightly oblique. The footwall and hanging wall damage zones consist of clusters of anastomosing deformation bands (Figure 4C) and isolated single deformation bands (Figure 4D). Deformation bands also form a small positive relief. The fault cores and deformation bands exhibit lighter colors than surrounding host rocks (Figure 4B–D) and in some cases an orange to red coloration is also observed.
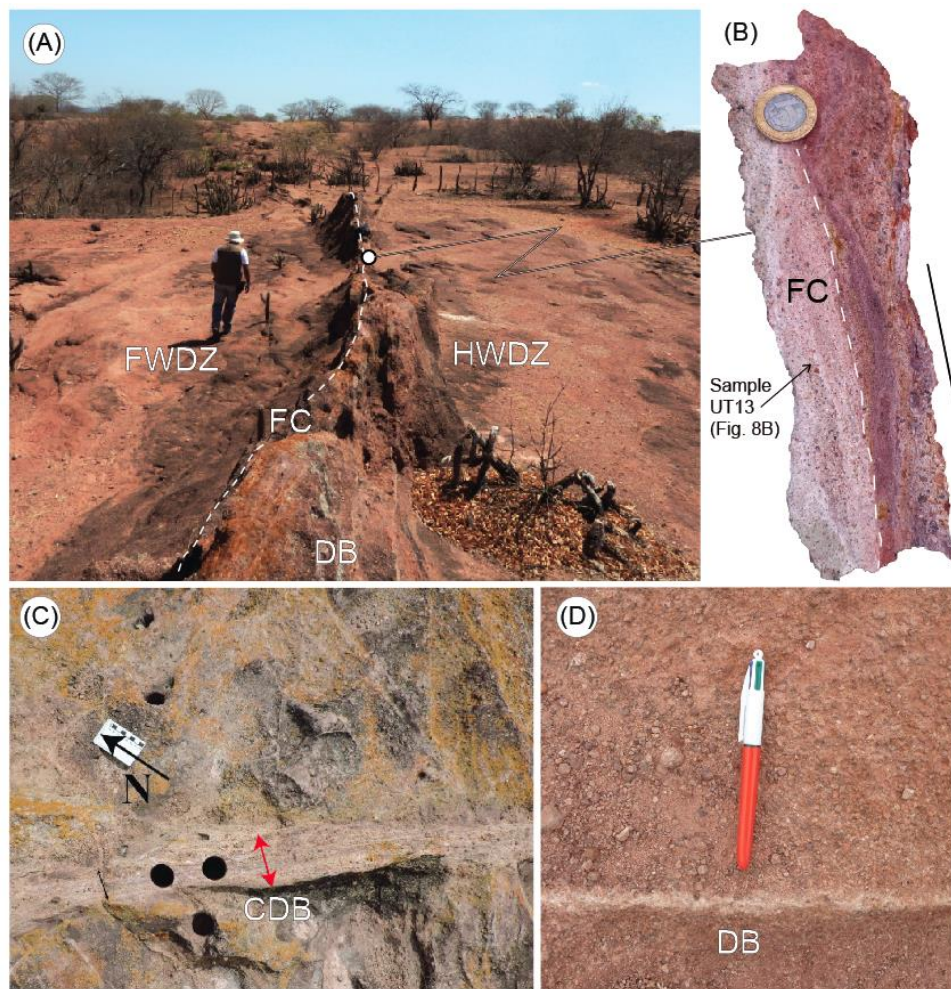
Figure 4. Field photographs showing the main structural features of studied fault zones in the Rio do Peixe basin. (**A**) Example of an extensional fault zone with m-scale offset showing positive relief with respect to the host sandstone, Site 2. The dotted line indicates the approximate position of the fault core. (**B**) Foliated fault core rock (sample UT13 in Table 1) showing light grey to red colors, Site 2. The diameter of the coin is ~2.5 cm. (**C**) Example of a 12.0 cm-thick cluster of deformation bands, in positive relief, developed in the fault damage zone, Site 4. The length of the white scale is ~8.0 cm. (**D**) Whitish single deformation band in positive relief developed in the damage zone, Site 2. The length of the pen is ~14.0 cm. Key: FWDZ—footwall damage zone; HWDZ—hanging wall damage zone; FC—fault core; DB—deformation band; CDB—cluster of deformation bands.

4.2. Petrography

4.2.1. Host Rock

The host rock comprises: (1) fine-grained sandstones with moderate sorting and angular grains (Figure 5A); and (2) coarse-grained, generally poorly sorted sandstones with sub-rounded grains (Figure 5B,C). Point, line and concave–convex grain contacts predominate, while floating and sutured grains are rare. These grain contacts indicate that the sandstones have moderate packing and shallow burial conditions. The sandstones are composed of feldspar, quartz, chert, metamorphic lithoclasts and opaque minerals, although the percentage of these minerals varies in each sample. In thin sections, feldspar is usually the most abundant constituent (~60%), followed by quartz (~40%), lithoclasts (up to 10%) and opaque minerals (~1%). Feldspar grains generally show microfractures and are often partially to completely dissolved, while quartz grains are generally intact. The sandstones vary from arkose to lithic arkose according to the Folk (1968) classification (Figure 3C). All analyzed samples commonly

exhibit primary intergranular porosity and, subordinately, secondary moldic porosity associated with the selective dissolution of feldspar grains (Figure 5E,F). Fracture porosity is also observed (Figure 5C), although fractures are mostly filled by clay minerals. In thin sections, visual porosity was observed to be 17% and 28% in fine and coarse sandstones, respectively. Generally, grains are coated by thin layers of clay minerals; these are even more abundant within intergranular pores and microfractures. In some samples, pores show shrinkage (Figure 5B,C). In rare cases, the porosity is almost entirely filled by clay minerals (Figure 5A).
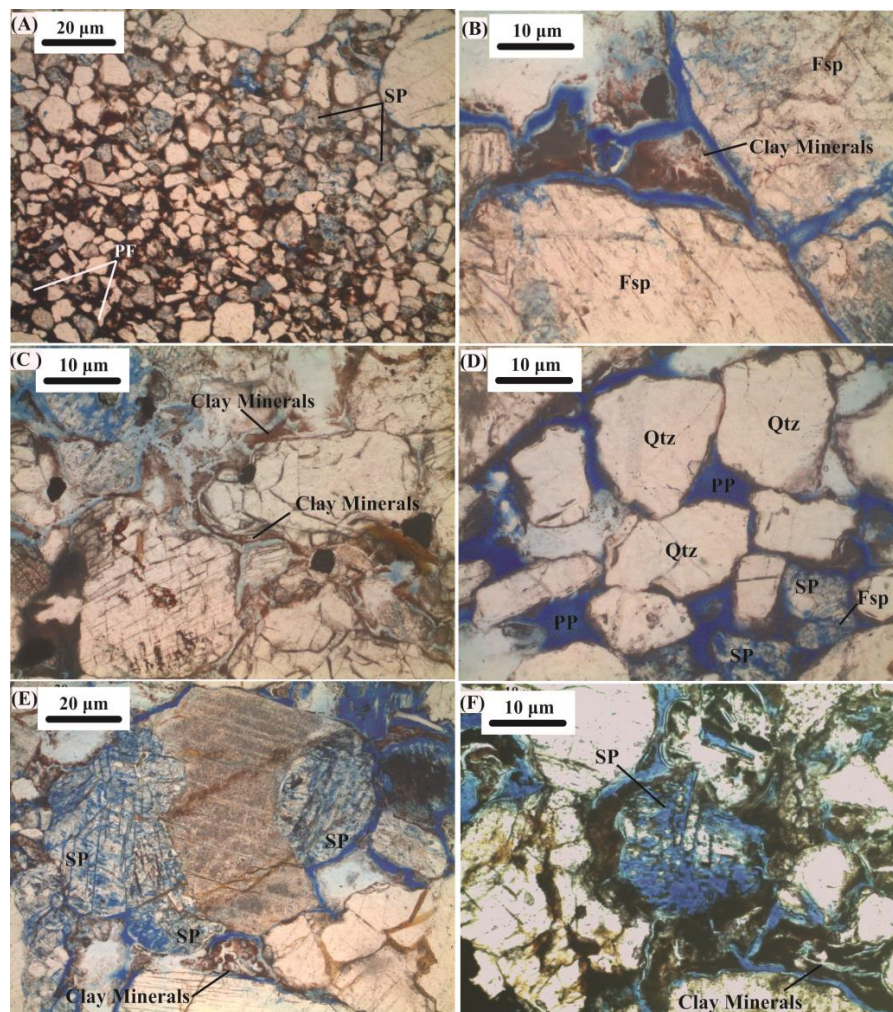

Figure 5. Optical microscopic images of the undeformed Rio do Peixe basin sandstones at Site 1. (**A**) Host rock, with very fine grains and abundant small pores which are frequently filled by clay minerals (pore filling, PF). The porosity is mainly secondary porosity (SP). (**B**) Coarse-grained sandstone showing sub-rounded grains and primary porosity, partially filled by smectite and illite. (**C**) Example of a feldspar clast dissolved and replaced by abundant clays. (**D**–**F**) show intergranular primary porosity (PP) between quartz grains (Qtz) and SP resulting from the dissolution of feldspar grains (Fsp).

4.2.2. Fault Rocks

The deformed sandstones show different degrees of deformation, most likely due to the amount of offset accommodated within the fault zones (Figure 6). The samples from single deformation bands exhibit a tight fabric and limited intergranular and secondary moldic (feldspar dissolution) porosity compared to the host rock (Figure 6A,B). The visual porosity inside the deformation bands is around 11%, i.e., lower than host rock samples. Intragranular fractures are common in quartz and feldspar

grains within the deformation bands (Figure 6C). In places, fractures are open and filled by fine-grained angular cataclastic material (Figure 6D).

　　Samples from fault cores exhibit a strong reduction in grain size with abundant fractions ranging from fine sand to silt (Figure 6E,F). In strong contrast to the undeformed host rock, fault core samples are clearly matrix-supported and very poorly sorted (Figure 6E,F). The brown colored, fine-grained matrix consists of crushed feldspar grains, in agreement with recent observations [34]. In the fault cores, the visual porosity determined using the optical microscope is practically zero due to the presence of the cataclastic matrix (Figure 6F).
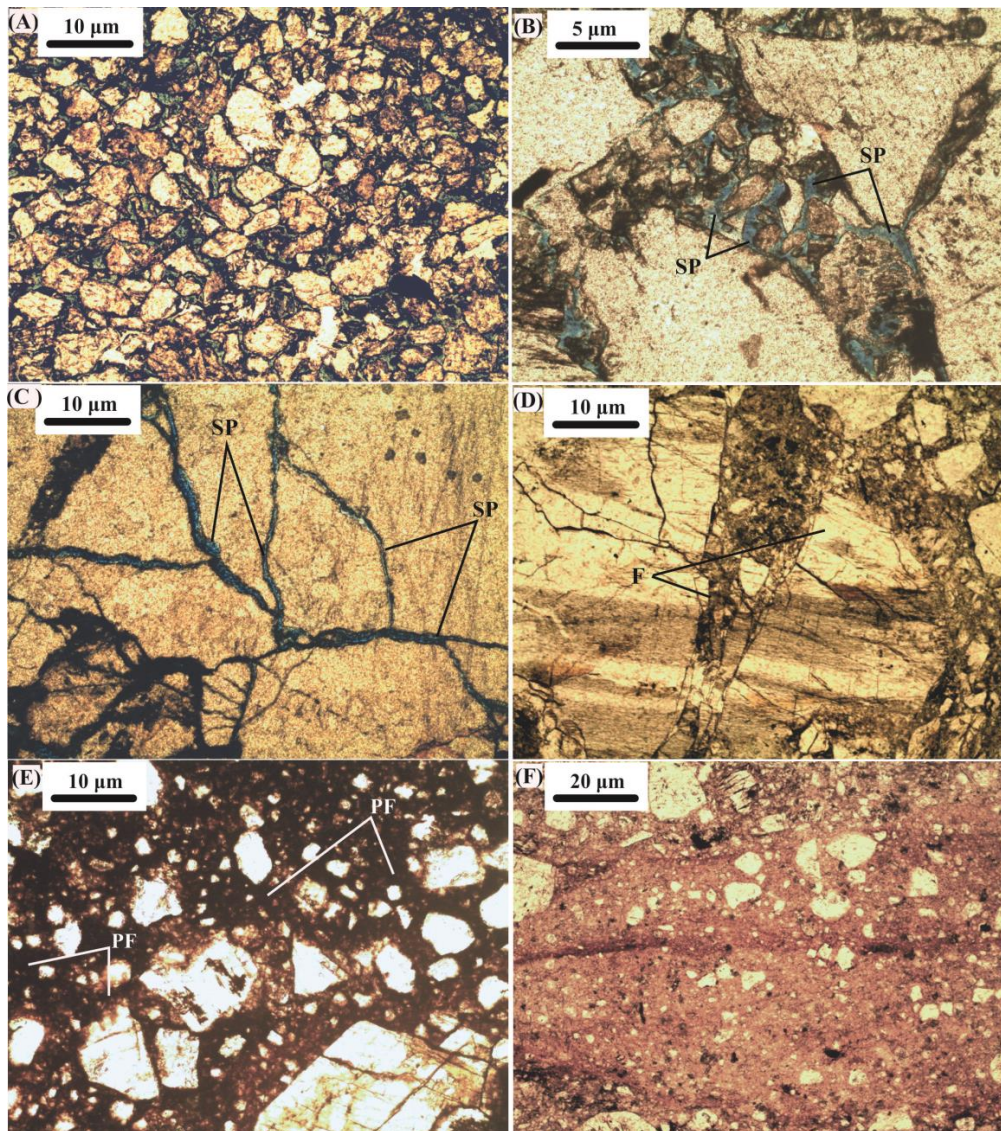

Figure 6. Fault rocks viewed under optical microscope. (**A**) Example of tight fabric in a deformation band within the damage zone, Site 2. (**B**) Detail of primary porosity filled by small angular clasts generated by the cataclasis process in a deformation band, Site 2. Note that feldspar grain dissolution is limited. (**C**) Secondary porosity (SP) developed by intragranular microfractures in a deformation band. (**D**) Detail of intragranular fractures filled by fine-grained angular cataclastic material in a small fault core. (**E**) Fine-grained matrix in the fault core resulting from high grain comminution, in which the pore space was completely destroyed, Site 3. (**F**) A high degree of cataclasis within the fault core, showing a dramatic reduction in grain size and porosity, Site 4. The brown crushed material in (**E**) and (**F**) mostly consist of very small feldspar grains developed during a cataclastic process cf. [34].

4.3. Clay Minerals

The clay minerals observed in the undeformed host hock are smectite, illite and subordinately kaolinite (Figure 7). These generally form a coating around clasts. The feldspars have a pore lining with an arrangement similar to the surrounding clay minerals, indicating growth into an open void (Figure 7A). The smectite and kaolinite exhibit a pore-filling texture (Figure 7B), while the illite shows a pore-lining geometry on quartz (Figure 7C). The smectite is marked by contraction fractures, likely due to sample drying (Figure 7D).
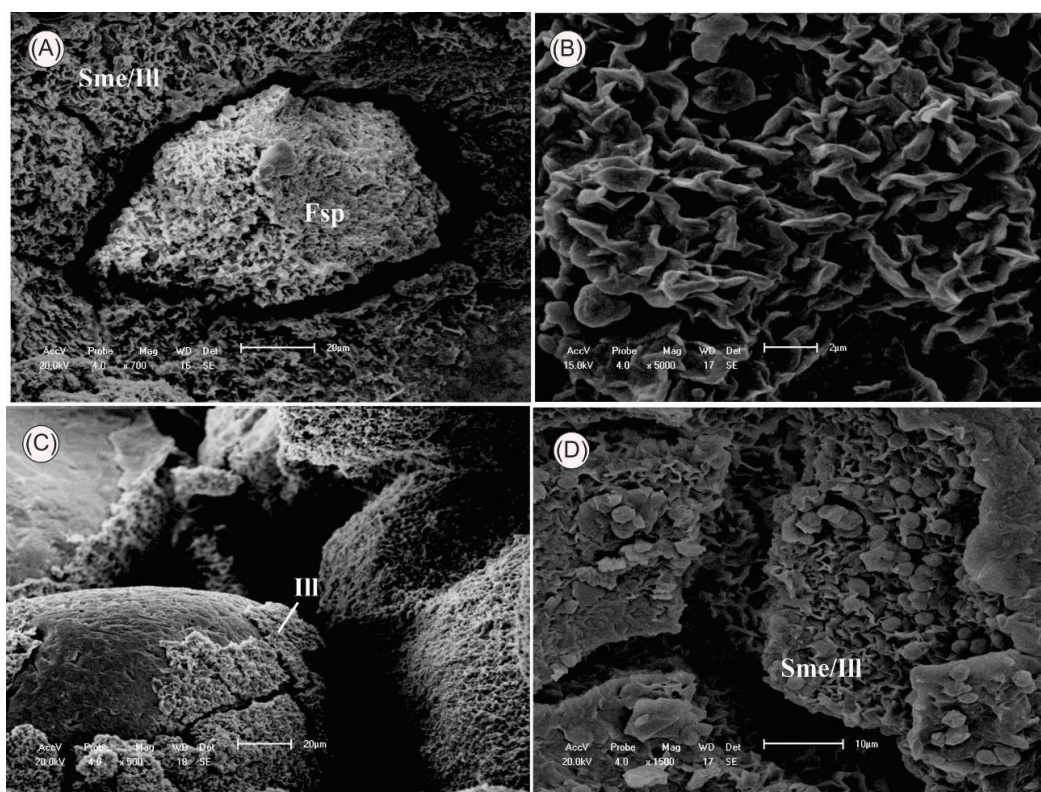

Figure 7. SEM images of clay minerals in undeformed sandstones. (**A**) Feldspar grain surrounded by fractured smectite. (**B**) Well developed smectite flakes inside a pore. (**C**) Pore-line illite coatings capping quartz grains. (**D**) Mixed layers of smectite and illite. Key: Sme—smectite; Fsp—feldspar; Ill—illite.

4.4. XRD Data

XRD bulk analysis was carried out on 10 samples as listed in Table 1. The results show that the main mineral phases identified in both undeformed and faulted sandstones are very similar (Figure 8A–C). Undeformed and faulted sandstones contain mostly quartz and feldspar (orthoclase, microcline and albite) and subordinately micas (Table 1). Hematite was only detected in three out of five undeformed sandstones, and was not detected in faulted samples. At low 2θ values, when clay minerals can be identified, undeformed sandstones show small spectral peaks (see enlargement in Figure 8A) which have a very low intensity (or are absent) in faulted sandstones (see enlargements in Figure 8B,C). Overall, semi-quantitative estimates based on XRD peak intensity, combined with thin section observations, indicate that the amount of clay minerals is systematically <1–2%. In three faulted samples (one of fault core rock and two of deformation bands), either no clay minerals were detected or insufficient material was available for clay fraction analysis (Table 1).

Table 1. Results of XRD analyses (bulk and clay fractions) performed in undeformed and faulted rocks from Sites 1, 2 and 4. (I-S: illite-smectite; DB: deformation bands). Sample labels are the same as Figures 8 and 9.

| Sample #	Site	Formation	Structural Domain	Bulk Mineralogy	Clay Mineralogy
SCP01	Site 1	Antenor Navarro	Host rock (fine conglomerate)	Quartz, feldspars, muscovite, hematite	Illite, smectite
SCP05	Site 1	Antenor Navarro	Host rock (fine sandstone)	Quartz, feldspars, muscovite, hematite	Illite, smectite
UT01	Site 2	Rio Piranhas	Host rock (fine sand)	Quartz, feldspars, muscovite	Illite, smectite, I-S mixed layers
UT11	Site 2	Rio Piranhas	Host rock (Fine sand)	Quartz, feldspars, muscovite	Illite, smectite, I-S mixed layers
UT13	Site 2	Rio Piranhas	Fault core (foliated cataclasite)	Quartz, feldspars, muscovite	Not analyzed (no enough clay)
UT14	Site 2	Rio Piranhas	Fault core (foliated cataclasite)	Quartz, feldspars	Illite, chlorite
SVEM1	Site 4	Antenor Navarro	Host rock (fine sandstone)	Quartz, feldspars, muscovite, hematite	Illite, smectite, I-S mixed layers
SVEF3	Site 4	Antenor Navarro	Damage zone (deformation band)	Quartz, feldspars, muscovite	No clay phase
SVEA1	Site 4	Antenor Navarro	Damage zone (cluster of DB)	Quartz, feldspars	Illite, smectite
SVEB2	Site 4	Antenor Navarro	Damage zone (cluster of DB)	Quartz, feldspars	No clay phase
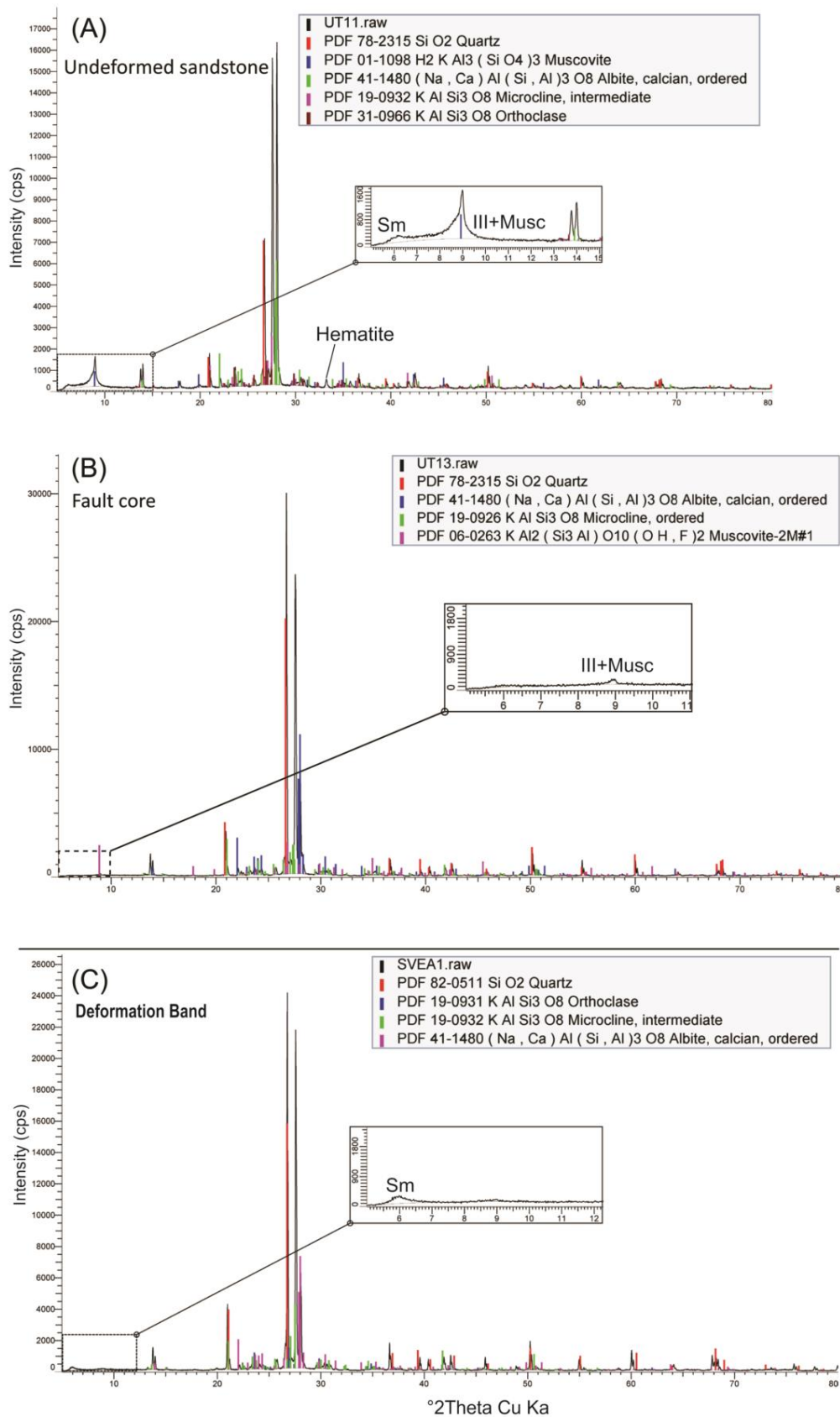
Figure 8. Examples of XRD analyses on bulk samples representative of undeformed sandstone (**A**), foliated cataclasite in fault core rock (**B**) and deformation band (**C**).

XRD analyses of clay fractions, performed on the six samples which had sufficient clay minerals in bulk analyses, indicate that the main types of clay minerals in both undeformed and faulted sandstones are smectite and subordinately illite (Figure 9), as indicated by the comparison between the XRD spectra of air-dried, glycolated and heated samples. Based on spectral peak intensities, in all the spectra the amount of illite was found to be less than that of smectite. Both illite and smectite occur as both distinct phases and mixed layers (Figure 9). In undeformed samples (Figure 9A–D) the spectral peaks of illite and smectite have greater intensities than in faulted samples (Figure 9E,F). Smectite is absent in the foliated fault-core rock (Figure 9E), which also shows the lowest amount of illite of all the analyzed samples; this is consistent with the non-weathered, whitish foliated cataclasites that are often observed in the field (e.g., Figure 4B) and the observed lack of clay minerals in thin sections (Figure 7E,F). A very small amount of chlorite is also observed in the fault core rock sample (Figure 9E).
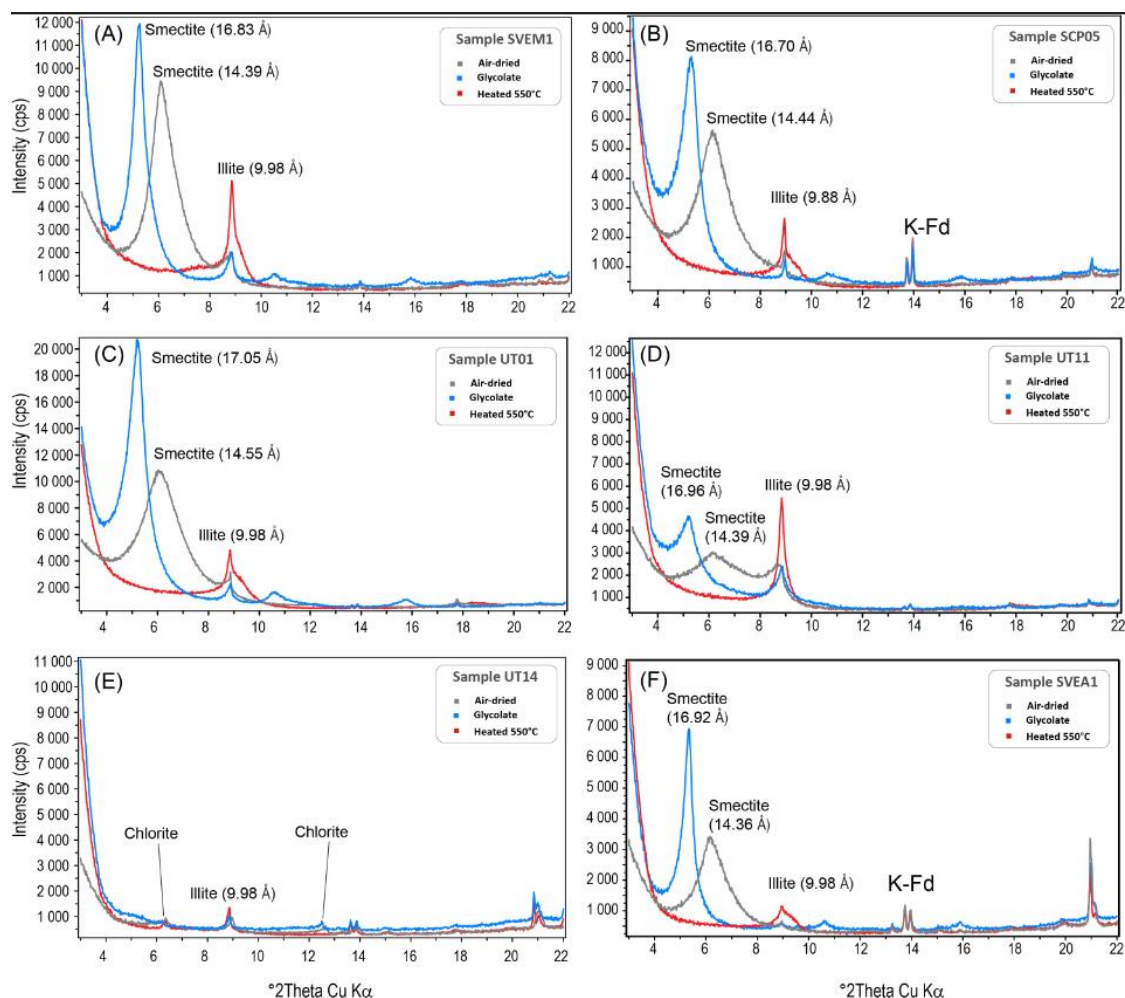

Figure 9. XRD diffractograms of aggregates of clay-size fractions of undeformed (**A**–**D**) and fault core (**E**) rocks, and a deformation band in a fault damage zone (**F**). Air-dried (in grey), heated at 550 °C (in red), and treated with ethylene glycol (in blue) conditions are shown.

5. Discussion

It is well known that the development of fault zones in sandstones can significantly modify fluid circulation pathways e.g., [12], thus influencing a variety of shallow diagenetic processes [21,24,38]. In this study, fault zones that developed in high-porosity arkosic sandstones are found to have the typical architecture described in other settings [9,24,38], being organized in a foliated fault-core surrounded by a damage zone hosting cataclastic deformation bands [34].

5.1. Origin of Clay Minerals

In the analyzed samples, illite and smectite were found to be the most abundant clay minerals (Figures 9 and 10) that typically occupy the spaces of the intergranular porosity of undeformed sandstones (Figures 5 and 7B). These phases are not easily distinguishable from one another under optical and electronic microscopy, however the results of XRD analysis on clay fractions indicate that illite and smectite occur both in mixed layers and as independent phases (Figure 9). Illite and smectite are among the most common clay minerals in sedimentary rocks. These minerals may form under diagenetic conditions at low pressure and temperature at near-surface conditions [5,8,24], typical of the shallow crust of the studied Rio do Peixe basin. The shallow burial depth during faulting (<1–2 km) is attested by the following conditions: (1) the syn-rift nature of extensional faults; (2) poorly lithified lithology; (3) the high-porosity framework in thin sections of undeformed sandstones; (4) the absence of high temperature mineral phases; and (5) the absence of quartz overgrowth in thin sections. Therefore, we interpret the occurrence of illite and smectite as the result of the partial weathering of K-feldspar and plagioclase grains during shallow early diagenesis under meteoric conditions [14]. This interpretation is strongly supported by the intense and selective dissolution of feldspar grains observed in thin sections (Figure 5). A detrital origin of the clay minerals in the studied samples is excluded since such clays are much more abundant in undeformed (porous) sandstones than in their faulted (non-porous) counterparts (Figure 10A–C), as discussed below.

5.2. Timing Between Clay Authigenesis and Faulting

The greater presence of clay minerals in the host rocks, and their scarcity or absence in the fault zone domains (both in thin sections and in X-ray diffractograms) indicates that, in the Rio do Peixe basin, clay authigenesis mostly occurred after the formation of faults. This interpretation implies that the studied fault zones acted as barriers to weathering meteoric fluids rather than preferential conduits, which is consistent with previously published data in similar lithologies. This hydraulic behavior is in agreement with pervasive grain fragmentation and cataclasis, as documented in thin sections (Figure 6), which provides a more compact, tight and impermeable fabric within the fault zones cf. [34]. Accordingly, when the studied extensional faults and deformation bands were formed at shallow burial depth, the rock volume incorporated into the fault zones could not provide an effective pathway for meteoric influx, thus compromising the process of clay authigenesis and limiting the development of clay phases. This is also consistent with: (1) the presence of Fe-oxides in the host rocks, and not in their faulted counterparts (Table 1); and (2) the intense reddish coloration of host rocks and the orange to whitish coloration of faulted rocks observed in the field (as shown schematically in Figure 3).

Therefore, we believe that no significant amount of detrital clays was present in the sandstone before deformation, due to their absence in faulted samples. If clay minerals were present in the host sandstones at the time of faulting, they would have certainly been incorporated into the fault zones, probably reducing the friction between grains and preventing (or at least hindering) both cataclasis [23,24] and the development of deformation bands. In summary, we suggest that when the diagenetic process of clay authigenesis occurred in the high-porosity undeformed sandstones, there was no significant porosity and sufficient permeability within the fault zones for meteoric fluid circulation and intense alteration of feldspars.

5.3. Evolutionary Model

Based on field observations and laboratory results, we propose the following evolutionary model for the generation of clay minerals after sediment deposition in the following sequence: (1) the syn- to post-sedimentary formation of extensional faults and deformation bands in poorly lithified sandstones, inducing localized grain compaction and early comminution within the fault zones; (2) the further evolution of failure and the generation of low-permeability cataclastic fault zones; (3) the beginning of the weathering process during shallow diagenesis and meteoric fluid circulation; (4) the selective

weathering and dissolution of feldspar grains in a semi-arid environment (as shown by moldic porosity in thin sections) and clay mineral authigenesis in the high-porosity undeformed sandstones and conglomerates; (5) the exhumation of faults during regional basin inversion and the formation of positive reliefs of fault zones (due to differential surface erosion) caused by a tight cataclastic fabric.
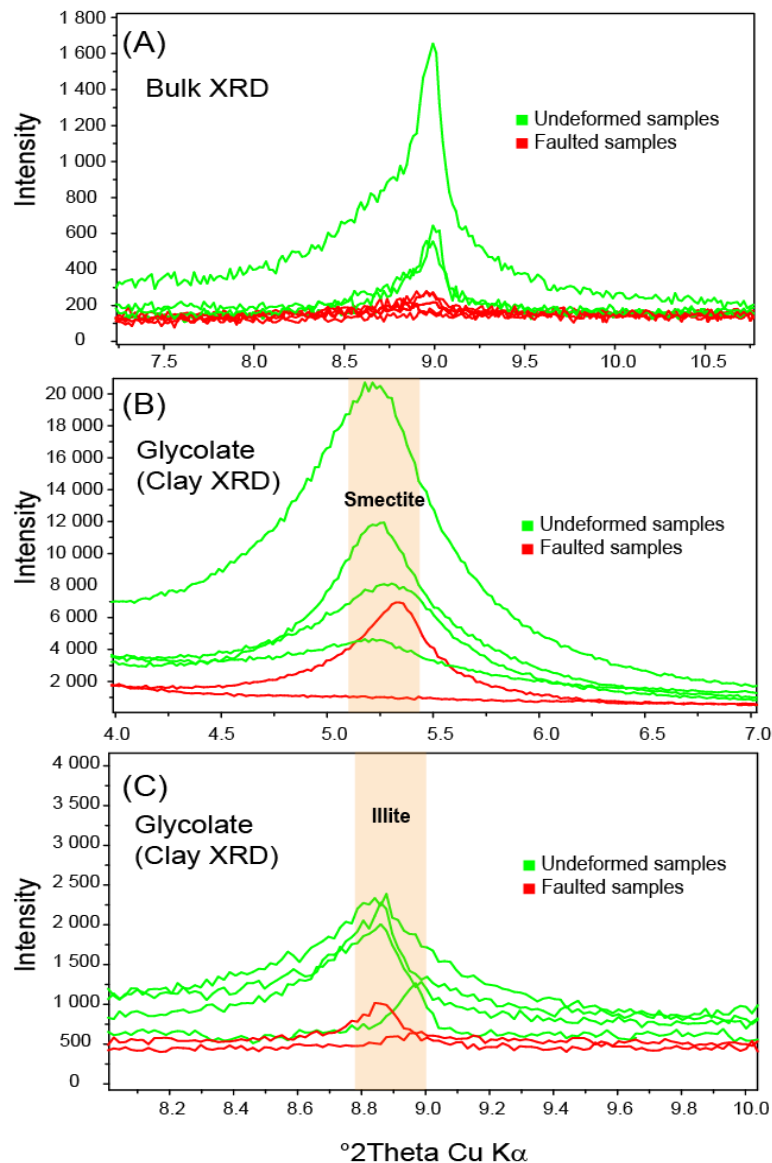

Figure 10. Summary diagrams showing a comparison between diffractograms of undeformed host rocks (green lines) and faulted rocks (red lines). (**A**) Bulk XRD analysis indicating that that the amount of clay minerals in the undeformed samples is higher than that in faulted samples. (**B**) The relative abundance of smectite in undeformed and faulted samples. (**C**) The relative abundance of illite in undeformed and faulted samples.

6. Conclusions

We studied clay mineral assemblages in faulted, high-porosity arkosic sandstone of the Rio do Peixe basin (northeast Brazil) to understand the role of faults in clay mineral authigenesis. We integrated field observations with analysis of microstructures, optical and scanning electron microscopy and XRD (bulk and clay-fraction) mineralogy. The results obtained in this study indicate the following conclusions:

(1)　The bulk mineralogy of the Rio do Peixe sandstone does not change significantly between the undeformed and faulted domains, consisting of lithic arkose with feldspar grains generally comprising >50%.

(2)　In both undeformed and faulted domains, clay minerals are <1–2% and consist of smectite and illite, and subordinately illite–smectite mixed layers. Despite the similar mineralogy, the amount of clay is systematically less in the faulted domain than in pristine rocks and in some cases is not observed at all.

(3)　Clay minerals in the studied arkosic sandstones most likely developed during feldspar weathering processes in a shallow meteoric environment. A detrital origin of clay is excluded in the analyzed sandstones and conglomerates.

(4)　Contrary to the results of other fault rock studies in similar lithologies, clay is found to be less abundant in the faulted domains (fault core and damage zone) than in the host rocks. We conclude that this is due to the tight fabric that developed in the faulted porous sandstone, which inhibited meteoric fluid circulation and clay mineral authigenesis.

We conclude that, contrary to several other faulted settings which have a high abundance of authigenic clays, the development of fault zones in high-porosity arkosic sandstone in semi-arid regions prevents the authigenesis of clay minerals. Consequently, clay authigenesis is more efficient in undeformed sandstones than faulted domains, which has important implications for oil and water reservoir quality in siliciclastic rocks and fault behavior in structurally complex settings.

Conflicts of Interest: The authors declare no conflicts of interest.

References

1.　Xi, K.; Cao, Y.; Liu, K.; Jahren, J.; Zhu, R.; Yuan, G.; Hellevang, H. Authigenic minerals related to wettability and their impacts on oil accumulation in tight sandstone reservoirs: An example from the Lower Cretaceous Quantou Formation in the southern Songliao Basin, China. *J. Asian Earth Sci.* **2018**. [CrossRef]

2.　Rice, J.R. Fault stress states, pore pressure distributions, and the weakness of the San Andreas Fault. In *International Geophysics*; Academic Press: Cambridge, MA, USA, 1992; pp. 475–503.

3.　Fisher, Q.J.; Knipe, R.J. Fault sealing processes in siliciclastic sediments. In Faulting, Fault Sealing and Fluid Flow in Hydrocarbon Reservoirs. *Geol. Soc. Spec. Publ.* **1998**, *147*, 117–134. [CrossRef]

4.　Haines, S.H.; Van der Pluijm, B.A.; Ikari, M.J.; Saffer, D.M.; Marone, C. Clay fabric intensity in natural and artificial fault gouges: Implications for brittle fault zone processes and sedimentary basin clay fabric evolution. *J. Geophys. Res.* **2009**, *114*, B05406. [CrossRef]

5.　Lander, R.H.; Bonnell, L.M. A model for fibrous illite nucleation and growth in sandstones. *AAPG Bull.* **2010**, *94*, 1161–1187. [CrossRef]

6.　Faulkner, D.R.; Jackson, C.A.L.; Lunn, R.J.; Schlische, R.W.; Shipton, Z.K.; Wibberley, C.A.J.; Withjack, M.O. A review of recent developments concerning the structure, mechanics and fluid flow properties of fault zones. *J. Struct. Geol.* **2010**, *32*, 1557–1575. [CrossRef]

7.   Balsamo, F.; Aldega, L.; De Paola, N.; Faoro, I.; Storti, F. The signature and mechanics of earthquake ruptures along shallow creeping faults in sediments. *Geology* **2014**, *42*, 435–438. [CrossRef]

8.   Buatier, M.D.; Cavailhes, T.; Charpentier, D.; Lerat, J.; Sizun, J.P.; Labaume, P.; Gout, C. Evidence of multi-stage faulting by clay mineral analysis: Example in a normal fault zone affecting arkosic sandstones (Annot sandstones). *J. Struct. Geol.* **2015**, *75*, 101–117. [CrossRef]

9.   Antonellini, M.; Aydin, A. Effect of Faulting on Fluid Flow in Porous Sandstones: Petrophysical Properties. *AAPG Bull.* **1994**, *78*, 355–377.

10. Rawling, G.C.; Goodwin, L.B.; Wilson, J.L. Internal architecture, permeability structure, and hydrologic significance of contrasting fault-zone types. *Geology* **2001**, *29*, 43–46. [CrossRef]

11. Eichhbl, P.; Taylor, W.L.; Pollard, D.D.; Aydin, A. Paleo-fluid flow and deformation in the Aztec Sandstone at the Valley of Fire, Nevada—Evidence for the coupling of hidrogeologic, diagenetic, and tectonic process. *GSA Bull.* **2004**, *116*, 1120–1136. [CrossRef]

12. Fossen, H.; Schultz, R.A.; Shipton, Z.K.; Mair, K. Deformation bands in sandstone: A review. *J. Geol. Soc.* **2007**, *164*, 755–769. [CrossRef]

13. Caine, J.S.; Minor, S.A. Structural and geochemical characteristics of faulted sediments and inferences on the role of water in deformation, Rio Grande Rift, New Mexico. *GSA Bull.* **2009**, *121*, 1325–1340. [CrossRef]

14. Vrolijk, P.; Van der Pluijm, B. Clay gouge. *J. Struct. Geol.* **1999**, *21*, 1039–1048. [CrossRef]

15. Gibson, R. Physical character and fluid-flow properties of sandstonederived fault gouge, in Structural Geology in Reservoir Characterization. *Geol. Soc. Spec. Publ.* **1998**, *127*, 87–93. [CrossRef]

16. Fisher, Q.; Knipe, R.J. The permeability of faults within siliclastic petroleum reservoirs of the North Sea and Norwegian Continental Shelf. *Mar. Pet. Geol.* **2001**, *18*, 1063–1081. [CrossRef]

17. Fossen, H.; Bale, A. Deformation bands and their influence on fluid flow. *AAPG Bull.* **2007**, *91*, 1685–1700. [CrossRef]

18. Rotevatn, A.; Torabi, A.; Fossen, H.; Braathen, A. Slipped deformation bands: A new type of cataclastic deformation bands in Western Sinai, Suez rift, Egypt. *J. Struct. Geol.* **2008**, *30*, 1317–1331. [CrossRef]

19. Eichhubl, P.; Davatzes, N.C.; Becker, S.P. Structural and diagenetic control of fluid migration and cementation along the Moab Fault, Utah. *AAPG Bull.* **2009**, *93*, 653–681. [CrossRef]

20. Balsamo, F.; Storti, F.; Salvini, F.; Lima, C.C. Structural and petrophysical evolution of extensional fault zones in low-porosity, poorly lithified sandstones of the Barreiras Formation NE Brazil. *J. Struct. Geol.* **2010**, *32*, 1806–1826. [CrossRef]

21. Balsamo, F.; Bezerra, F.H.; Vieira, M.; Storti, F. Structural control on the formation of iron oxide concretions and Liesegang bands in faulted, poorly lithified Cenozoic sandstones of the Paraiba basin, Brazil. *Bulletin* **2013**, *125*, 913–931. [CrossRef]

22. Williams, J.N.; Toy, V.G.; Massiot, C.; McNamara, D.D.; Wang, T. Damaged beyond repair? Characterising the damage zone of a fault late in its interseismic cycle, the Alpine Fault, New Zealand. *J. Struct. Geol.* **2016**, *90*, 76–94. [CrossRef]

23. Hoffman, U.; Endell, K.; Wilm, M.D. Kristallstruktur und Quellung von Montmorillonit. *Z. Kristallogr. Cryst. Mater.* **1933**, *86*, 340–348. [CrossRef]

24. Solum, J.G.; Davatzes, N.C.; Lockner, D.A. Fault-related clay authigenesis along the Moab Fault: Implications for calculations of fault rock composition and mechanical and hydrologic fault zone properties. *J. Struct. Geol.* **2010**, *32*, 1899–1911. [CrossRef]

25. Van der Pluijm, R. Out-of-Plane Bending of Masonry: Behaviour and Strength Eindhoven. Ph.D. Thesis, Technische Universiteit Eindhoven, Eindhoven, The Neitherlands, 1999.

26. Solum, J.G.; Van der Pluijm, B.A.; Peacor, D.R. Neocrystalization, fabrics and age of clay minerals from an exposure of the Moab Fault, Utah. *J. Struct. Geol.* **2005**, *27*, 1563–1576. [CrossRef]

27. Sénant, J.; Popoff, M. Early Cretaceous extension in northeast Brazil related to the South Atlantic opening. *Tectonophysics* **1991**, *198*, 35–46. [CrossRef]

28. Matos, R.M.D. The Northeast Brazilian Rift System. *Tectonics* **1992**, *11*, 766–791. [CrossRef]

29. Françolin, J.B.L.; Cobbold, P.R.; Szatmari, P. Faulting in the early Cretaceous Rio do Peixe basin (NE Brazil) and its significance for the opening of the Atlantic. *J. Struct. Geol.* **1994**, *16*, 647–661. [CrossRef]

30. De Castro, D.L.; De Oliveira, D.C.; Gomes Castelo Branco, R.M. On the tectonics of the Neocomian Rio do Peixe Rift Basin, NE Brazil: Lessons from gravity, magnetics, and radiometric data. *J. South. Am. Earth Sci.* **2007**, *24*, 184–202. [CrossRef]

31. Albuquerque, J.P.T. *Inventário Hidrogeológico do Nordeste*; Folha 15; Sudene, Divisão de Documentação: Recife, Brazil, 1970; p. 187.

32. Lima, M.R.; Coelho, M.P.C.A. Estudo palinológico da sondagem de Lagoa do Forno Bacia do Rio do Peixe Cretáceo do Nordeste do Brasil. São Paulo. *Bol. IG-USP Sci.* **1987**, *18*, 67–83.

33. Córdoba, V.C.; Antunes, A.F.; Jardim de Sá, E.F.; Nunes da Silva, A.; Sousa, D.C.; Lins, F.A.P.L. Análise estratigráfica e estrutural da Bacia do Rio do Peixe Nordeste do Brasil: Integração de dados a partir do levantamento sísmico pioneiro 0295_rio_do_peixe_2d. *Bol. Geoci. Petrobras* **2008**, *16*, 53–68.

34. Nicchio, M.A.; Nogueira, F.C.C.; Balsamo, F.; Souza, J.A.B.; Carvalho, B.R.B.; Bezerra, F.H.R. Development of cataclastic foliation in deformation bands in feldspar-rich conglomerates of the Rio do Peixe Basin, NE Brazil. *J. Struct. Geol.* **2018**, *107*, 132–141. [CrossRef]

35. Nogueira, F.C.C.; Marques, F.O.; Bezerra, F.H.R.; de Castro, D.L.; Fuck, R.A. Cretaceous intracontinental rifting and post-rift inversion in NE Brazil: Insights from the Rio do Peixe Basin. *Tectonophysics* **2015**, *644*, 92–107. [CrossRef]

36. Araujo, R.E.B.; Bezerra, F.H.R.; Nogueira, F.C.C.; Balsamo, F.; Carvalho, B.R.B.M.; Souza, J.A.B.; Sanglard, J.C.D.; de Castro, D.L.; Melo, A.C.C. Basement control on fault formation and deformation band damage zone evolution in the Rio do Peixe Basin, Brazil. *Tectonophysics* **2018**, *745*, 117–131. [CrossRef]

37. Folk, R.L. *Petrology of Sedimentary Rocks*; Hemphill Publishing Company: Austin, TX, USA, 1968; p. 182.

38. Balsamo, F.; Storti, F.; Grocke, D. Fault-related fluid flow history in shallow marine sediments from carbonate concretions, Crotone Basin, south Italy. *J. Geol. Soc.* **2012**, *169*, 613–626. [CrossRef]